Covariant confinement model for the study of the properties of light mesons

L. S. Celenza, Bo Huang, Huangsheng Wang, and C. M. Shakin*
Department of Physics and Center for Nuclear Theory, Brooklyn College of the City University of New York, Brooklyn, New York 11210
(Received 21 January 1999; revised manuscript received 24 March 1999; published 29 June 1999)

We continue our studies of a relativistic quark model that includes a covariant model of confinement. [In the absence of the confinement model, our model reduces to the SU(3)-flavor version of the Nambu–Jona-Lasinio (NJL) model.] In previous works we have studied the radial excitations of the pion, η-η' mixing, and ω-ϕ mixing. Here we extend our work to study the K mesons of the pseudoscalar, vector, and scalar nonets. In addition, we provide some preliminary analysis of the $^3P_1$ and $^1P_1$ axial-vector nonets and develop a formalism that enables us to consider $^3P_1$-$^1P_1$ mixing of the strange axial-vector mesons. That is accomplished by adding interactions to the NJL Lagrangian that contain gradients of the quark field. Once the parameters of the model are fixed by fitting the energies of the $\omega(782)$, $\omega(1420)$, $K(495)$, and $\phi(1020)$, we find the model has significant predictive power. For example, the masses of the $K^*(892)$, $K_0^*(1430)$, and $a_1(1260)$ are predicted correctly. For the pseudoscalar nonet we find nineteen states below 2 GeV and for the vector nonet we have eleven states with mass less than 2 GeV. On the whole, the pattern of radial excitations of the various mesons is reproduced in our model. [S0556-2813(99)01108-5]

PACS number(s): 12.39.Ki, 14.40.−n, 14.65.Bt

I. INTRODUCTION

In a number of recent works [1–5] we have been developing a relativistic quark model that includes a covariant model of confinement. The Lagrangian of the model is

$$\mathcal{L}=\overline{q}(i\not\partial-m^0)q+\frac{G_S}{4}\sum_{i=0}^{8}[(\overline{q}\lambda^i q)^2+(\overline{q}i\gamma_5\lambda^i q)^2]$$
$$-\frac{G_V}{4}\sum_{i=0}^{8}[(\overline{q}\gamma^\mu\lambda^i q)^2+(\overline{q}\gamma^\mu\gamma_5\lambda^i q)^2]+\mathcal{L}_{\rm conf}, \tag{1.1}$$

where $\mathcal{L}_{\rm conf}$ denotes our model of confinement. In Eq. (1.1) m^0 is the current quark mass matrix, $m^0=\mathrm{diag}(m_u^0,m_d^0,m_s^0)$, the λ_i $(i=1,\ldots,8)$ are the Gell-Mann matrices, and $\lambda_0=\sqrt{2/3}I$, with I being the unit matrix in flavor space. In some calculations we have supplemented the Lagrangian of Eq. (1.1) with the 't Hooft interaction [6]. We remark that in the absence of our model of confinement, our Lagrangian is that of the Nambu–Jona-Lasinio (NJL) model [6].

In Ref. [1], we studied ω-ϕ and η-η' mixing and the radial excitations of these mesons. Reference [2] was concerned with the radial excitations of the pion and included a detailed treatment of π-a_1 mixing. Application was made to the decay of the $\pi(1300)$ to the $\pi+\sigma$ and $\pi+\rho$ channels. Reference [3] concerned the form of the T matrices of our model. With the confinement model in place, it was shown that the T matrix is represented only in terms of bound states, as might be expected. That work also contains a rather detailed discussion of meson-quark vertex functions of the confining model in the presence of singlet-octet and pseudoscalar–axial-vector mixing. In Refs. [4] and [5] we calculated the rates for the decays $\pi^0\to\gamma\gamma$, $\eta\to\gamma\gamma$, and $\eta'\to\gamma\gamma$ with satisfactory results. In the present study we extend our analysis to the strange mesons, which requires that we consider quarks and antiquarks of different constituent mass.

Our work is organized as follows. In Sec. II we comment on our treatment of confinement. In Sec. III we discuss the pseudoscalar nonet. In Sec. IV, we provide a short discussion concerning the choice of parameters made for this work. In Sec. V we discuss the vector nonet of states, using ideal mixing for the ϕ and ω mesons. In Sec. VI, we consider the scalar nonet of states and in Sec. VII we describe the $^3P_1$ and $^1P_1$ nonets of axial-vector mesons and $^3P_1$-$^1P_1$ mixing, as that mixing appears in the NJL model. Since the standard NJL interaction hardly affects $^1P_1$ states, in Sec. VIII we consider an extended NJL model, with an additional chirally-symmetric interaction that acts in $^1P_1$ states. Finally, Sec. IX contains some further discussion and conclusions.

II. MODEL OF CONFINEMENT

For Euclidean-space calculations we may write

$$\mathcal{L}_{\rm conf}(x)=\int d^4y\,\overline{q}(x)\gamma^\mu q(x)V^C(x-y)\overline{q}(y)\gamma_\mu q(y), \tag{2.1}$$

where, in momentum-space, V^C describes four-momentum transfer. However, for the Minkowski-space calculations reported here, we find it useful to neglect energy transfer by the confining field in the meson rest frame. For example, if we start with $V^C(r)=\kappa r\exp[-\mu r]$ and form the Fourier transform, we have

$$V^C(\vec{k}-\vec{k}')=-8\pi\kappa\left[\frac{1}{[(\vec{k}-\vec{k}')^2+\mu^2]^2}-\frac{4\mu^2}{[(\vec{k}-\vec{k}')^2+\mu^2]^3}\right]. \tag{2.2}$$

*Electronic address: CASBC@CUNYVM.CUNY.EDU

TABLE I. Psuedoscalar mesons. The pion states designated as $n\ ^1S_0$ have little pseudoscalar–axial-vector mixing [2]. Here $G_S = 12.46\ \mathrm{GeV}^{-2}$ for states other than the $\pi(138)$. Also, $\kappa = 0$ for the $\pi(138)$, and $\kappa = 0.0575\ \mathrm{GeV}^2$ for all other states. We use $\mu = 0.01$ GeV and $\Lambda_3 = 0.622$ GeV.

Meson	Mass (Expt.) [MeV]	Mass (Theory) [MeV]	Spectroscopic character
$\pi(138)$	π^0:134.97°64±0.0006 $\pi^{\pm}$:139.56995±0.00035	138	$1\ ^1S_0$
$\pi(1300)$	1300±100	1202[b]	mixed
		1400	$2\ ^1S_0$
		1539	mixed
$\pi(1800)$	1795±10[a]	1746	$3\ ^1S_0$
		1805	mixed
$K(495)$	$K^{\pm}$:493.677±0.016 K^0:497.672±0.031	495	$1\ ^1S_0$
$K(1460)$[a]	1400–1460	1557	$2\ ^1S_0$
$K(1830)$[a]	~1830	1879	$3\ ^1S_0$

[a]Needs confirmation.
[b]See Ref. [2] for a detailed study of this state.

Here μ is a small parameter used to soften the infrared singularities of V^C. If μ is small enough, the potential approximates a linear potential with ''string tension'' κ over the range of r relevant to our problem. The potential of Eq. (2.2) may be put in a covariant form [2], if we use the four-vectors $\hat{k}^\mu$ and $\hat{k}'^\mu$, where

$$\hat{k}^\mu(P) = k^\mu - \frac{(k\cdot P)P^\mu}{P^2} \tag{2.3a}$$

and

$$\hat{k}'^\mu(P) = k'^\mu - \frac{(k'\cdot P)P^\mu}{P^2}, \tag{2.3b}$$

since, when $\vec{P}=0$, we have $\hat{k}^\mu = [0,\vec{k}]$ and $\hat{k}'^\mu = [0,\vec{k}']$.

The calculation of confining vertex functions using Eq. (2.2), and the calculation of vacuum polarization integrals that incorporate such vertex functions, is described in detail in Refs. [1–5] and we do not repeat that material here. We note that the equations for the vertex functions do not require a cutoff. In our calculation of the vertex functions we have used momentum variables with $k_{\max} \simeq 2$–4 GeV and are, therefore, able to describe states with many nodes. The regulator for the (divergent) vacuum polarization integrals, Λ_3, is such that $|\vec{k}| \leq \Lambda_3$. Here we have used $\Lambda_3 = 0.622$ GeV. For that value, the vacuum polarization integrals have the correct spectral representation up to $P^2 = 4\ \mathrm{GeV}^2$. If we wish to calculate at larger values of P^2, we need to increase Λ_3. Our results are stable when such an increase is made, however, the coupling constants of the model have to be readjusted to produce the same spectrum of states.

III. THE PSEUDOSCALAR NONET

Since we have studied the radial excitations of the pion, including pseudoscalar–axial-vector mixing, in some detail

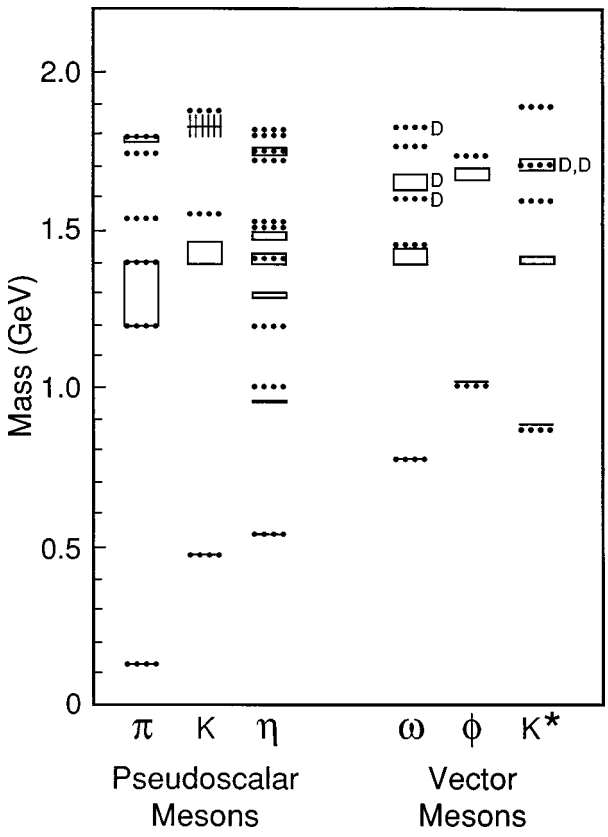

FIG. 1. Mass values for the mesons of the pseudoscalar and vector nonets are shown. The horizontal lines, rectangular boxes, and crosshatched regions show experimental values taken from Ref. [8]. The dotted lines represent the mass values calculated in this work. A small D is placed near those states that are calculated as D states or are so assigned in Table 12.2 of Ref. [8].

[2], we only comment upon the results here. In the confining field, considered in isolation, we find a series of doublets. One state of each doublet corresponds to the pseudoscalar vertex $i\gamma^5$ and the other corresponds to the axial-vector vertex $\gamma^0\gamma^5$, when $\vec{P}=0$. When we include the NJL interaction, one member of each doublet moves down in energy. The member of each doublet that moves down in energy to the greatest degree shows little mixing and can be identified as either the $\pi(1S)$, the $\pi(2S)$, or the $\pi(3S)$ state. The other three states exhibit significant mixing. (The details of our calculation for the pion and its radial excitations are given in Ref. [2].) For the results of the calculations made in this work, see Table I and Fig. 1.

In Ref. [1] we studied η-η' mixing and the radial excitations of that system of states. In that case, we included both singlet-octet and pseudoscalar–axial-vector mixing, leading to the study of quark T matrices of dimension four. The general form of the equation for the T matrix is

$$(1-GJ)T = -G. \tag{3.1}$$

The form of the matrices G and J may be found in the Appendix of Ref. [7]. [Note, however, that the sign of our func-

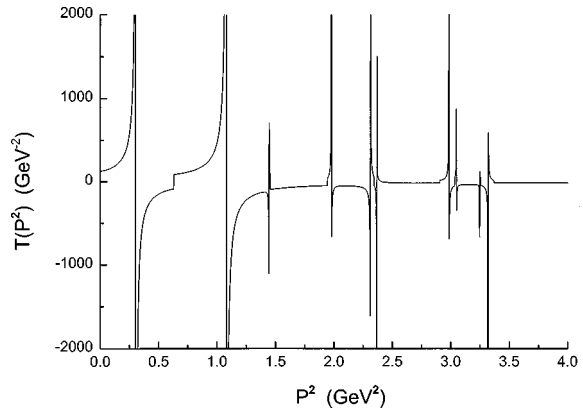

FIG. 2. The eigenvalue of the largest magnitude for the T matrix calculated in our study of the η-η' system. We find states with the energies 0.551, 1.039, 1.204, 1.406, 1.530, 1.543, 1.726, 1.749, 1.813, and 1.819 GeV, when the parameters of Table II are used.

tions $J^{PA}(P^2)$ and $J^{AA}(P^2)$ is the opposite of that used in Ref. [7].] The T matrix of Eq. (3.1) has singularities at the energies of the bound states of the quark and antiquark. In Fig. 2 we show the eigenvalue of the T matrix with the largest magnitude that is found at each value of P^2. (The calculations reported here differ from those of Ref. [1], since we now use $m_s=565$ MeV, rather than the value 480 MeV used in that work. We have also used $\mu=0.01$ GeV rather than the value $\mu=0.02$ GeV used previously.) In Fig. 2 we see ten states below 2.0 GeV. The mass values of these states are shown in Fig. 1 as dotted lines. The calculated energies are 0.551, 1.039, 1.204, 1.406, 1.530, 1.543, 1.726, 1.749, 1.803, and 1.819 in GeV units. We have used $G_S=12.46$ GeV^2 for the strength of the interaction in the octet states and G_S-δ for the strength in the singlet states. In this work we use $\delta=2.0$ GeV^{-2}, rather than the value of 4.0 GeV^{-2} used in Ref. [1]. (Details of these calculations may be found in that reference.)

We now turn to a study of the K meson. In this case, we have not included pseudoscalar–axial-vector mixing, so that we only have to generalize our calculations of the vertex functions and polarization functions, $\overline{\Gamma}_5(P,k)$ and $J^{PP}(P^2)$, to the case of different mass values for the up, down, and strange quarks. (Here, we take $m_u=m_d$.) To carry out this program, we define

$$\Lambda_a^{(+)}(\vec{k})=\frac{\not{k}_a+m_a}{2m_a} \tag{3.2}$$

and

$$\Lambda_b^{(-)}(-\vec{k})=\frac{\tilde{\not{k}}_b+m_b}{2m_b}, \tag{3.3}$$

with $k_a^\mu=[E_a(\vec{k}),\vec{k}]$ and $\tilde{k}_b^\mu=[-E_b(\vec{k}),\vec{k}]$. Here $E_a(\vec{k})=[\vec{k}^2+m_a^2]^{1/2}$, etc. The vertex function for pseudoscalar mesons is given by the equation

$$\overline{\Gamma}_{5,ab}(P,k)=\gamma_5-i\int\frac{d^4k'}{(2\pi)^4}[\gamma^\rho S_a(P/2+k')\overline{\Gamma}_{5,ab}(P,k')\times S_b(-P/2+k')\gamma_\rho]V^C(k-k'), \tag{3.4}$$

where $S_a(P)=[\not{P}-m_a+i\epsilon]^{-1}$, etc. The analysis proceeds by multiplying Eq. (3.4) from the left by $\gamma_5\Lambda_a^{(+)}(\vec{k})$ and from the right by $\Lambda_b^{(-)}(-\vec{k})$ and forming the trace. If we neglect coupling between $\Gamma_{5,ab}^{+-}$ and $\Gamma_{5,ab}^{-+}$, we find

$$\Gamma_{5,ab}^{+-}(P^0,|\vec{k}|)=1-\int\frac{d^3k'}{(2\pi)^3}\frac{B(\vec{k},\vec{k}')\Gamma_{5,ab}^{+-}(P^0,|\vec{k}'|)V^C(\vec{k}-\vec{k}')}{P^0-E_a(\vec{k}')-E_b(\vec{k}')}, \tag{3.5}$$

with

$$\begin{aligned}B(\vec{k},\vec{k}')=&\frac{1}{2E_a(\vec{k}')E_b(\vec{k}')[m_am_b+E_a(\vec{k})E_b(\vec{k})+\vec{k}^2]}\{m_am_b[E_a(\vec{k})E_b(\vec{k}')+E_b(\vec{k})E_a(\vec{k}')+2\vec{k}\cdot\vec{k}'-2E_a(\vec{k}')E_b(\vec{k}')\\&-2E_a(\vec{k})E_b(\vec{k})-2\vec{k}^2-2\vec{k}'^2]+m_b^2[E_a(\vec{k})E_a(\vec{k}')-\vec{k}\cdot\vec{k}']+m_a^2[E_b(\vec{k})E_b(\vec{k}')-\vec{k}\cdot\vec{k}']\\&-2[(E_a(\vec{k})E_b(\vec{k})+\vec{k}^2)(E_a(\vec{k}')E_b(\vec{k}')+\vec{k}'^2)]-2m_a^2m_b^2\}.\end{aligned} \tag{3.6}$$

Note that $\Gamma_{5,ab}^{-+}(P,k)$ satisfies the equation

$$\Gamma_{5,ab}^{-+}(P^0,|\vec{k}|)=1+\int\frac{d^3k'}{(2\pi)^3}\frac{B(\vec{k},\vec{k}')\Gamma_{5,ab}^{-+}(P^0,|\vec{k}'|)V^C(\vec{k}-\vec{k}')}{P^0+E_a(\vec{k}')+E_b(\vec{k}')}. \tag{3.7}$$

These equations are much simpler when $m_a = m_b$. In that case, we have

$$\Gamma_5^{+-}(P^0,|\vec{k}|) = 1 - \int \frac{d^3k'}{(2\pi)^3}\left[\frac{m^2 - 2E(\vec{k})E(\vec{k}')}{E(\vec{k})E(\vec{k}')}\right] \times \frac{\Gamma_5^{+-}(P^0,|\vec{k}'|)V^C(\vec{k}-\vec{k}')}{P^0 - 2E(\vec{k}')} \tag{3.8}$$

and

$$\Gamma_5^{-+}(P^0,|\vec{k}|) = 1 + \int \frac{d^3k'}{(2\pi)^3}\left[\frac{m^2 - 2E(\vec{k})E(\vec{k}')}{E(\vec{k})E(\vec{k}')}\right] \times \frac{\Gamma_5^{-+}(P^0,|\vec{k}'|)V^C(\vec{k}-\vec{k}')}{P^0 + 2E(\vec{k}')}. \tag{3.9}$$

We see from Eqs. (3.8) and (3.9) that these are significant relativistic kinematic corrections to $V^C(\vec{k}-\vec{k}')$ that are represented by the terms in square brackets.

For $m_a \neq m_b$, we define the polarization function

$$-iJ_{ab}^{PP}(P) = -2n_c \int \frac{d^4k}{(2\pi)^4} \mathrm{Tr}[iS_a(P/2+k) \times i\overline{\Gamma}_{5,ab}(P,k) iS_b(-P/2+k) i\gamma_5], \tag{3.10}$$

where the factor of 2 arises from the flavor trace. We obtain

$$J_{ab}^{PP}(P^2) = -2n_c \int \frac{d^3k}{(2\pi)^3} \frac{[E_a(\vec{k})E_b(\vec{k}) + \vec{k}^2 + m_a m_b]}{P^0 - E_a(\vec{k}) - E_b(\vec{k})} \times \frac{\Gamma_{5,ab}^{+-}(P^0,|\vec{k}|)}{E_a(\vec{k})E_b(\vec{k})}, \tag{3.11}$$

if we neglect the contribution from the $\Gamma_{5,ab}^{-+}(P,k)$ term. Note, however, that for the study of the $\pi(138)$, we use the form [2]

$$J^{PP}(P^2) = -4n_c \int \frac{d^3k}{(2\pi)^3}\left[\frac{1}{P^0 - 2E(\vec{k})} - \frac{1}{P^0 + 2E(\vec{k})}\right], \tag{3.12}$$

since we have neglected confinement in that case.

For the kaon and its radially-excited states, the mass values may be obtained from the solution of the equation

$$G_S^{-1} - J_{us}^{PP}(P^2) = 0, \tag{3.13}$$

where now $m_a = m_u$ and $m_b = m_s$. The results of our calculations for the K meson are given in Table I, where we also provide mass values for the pion and its radial excitations. We note that the mass of the $K(1460)$ and $K(1830)$ are quite uncertain and these states need further confirmation [8]. However, we do see that after fitting the mass of the $K(495)$, we obtain the 2^1S_0 and 3^1S_0 states in the vicinity of the $K(1460)$ and $K(1830)$ states.

TABLE II. Parameters used in this work—see Sec. IV. The first three of these parameters are not varied when fitting data. The parameters G_K and G_{KA} are used in the study of $^3P_1$-$^1P_1$ mixing of strange axial-vector mesons. [See Eq. (8.1).] The parameter δ is used in the study of η-η' mixing.

$\mu = 0.010$ GeV
$\Lambda_3 = 0.622$ GeV
$m_u = 0.364$ GeV
$m_s = 0.565$ GeV
$\kappa = 0.055$ GeV^2
$G_V = 12.46$ GeV^{-2}
$G_S = 12.46$ GeV^{-2}
$\delta = 2.0$ GeV^{-2}
$G_K = 78.13$ GeV^{-2}, $G_{KA} = 8.00$ GeV^{-2}

IV. CHOICE OF PARAMETERS

In this section, we indicate how we have chosen the parameters for our calculation. There are ten parameters, but we only search for the best values of seven of these: G_S, G_V, κ, G_K, G_{KA}, δ, and m_s. We fix $m_u = m_d = 0.364$ GeV, $\Lambda_3 = 0.622$ GeV, and $\mu = 0.010$ GeV. (The value of 0.364 GeV for the mass of the up and down quarks was used in the extensive study reported in Ref. [7] and we adopt that value here.) Ideally, we should solve the Bethe-Salpeter equation in conjunction with the Schwinger-Dyson equation to obtain the quark self-energy. We have carried out that program in one of our papers using a Euclidean momentum space [9]. Since we perform our calculations in Minkowski space, that program is extremely difficult to implement. Therefore, we adopt a more phenomenological approach in our Minkowski-space calculations and use constant values for the constituent quark masses. We note that solutions in Euclidean space of the coupled Schwinger-Dyson and Bethe-Salpeter equations have been made using the global color model [10]. The constituent quark masses found in that model are rather similar to the ones used here, $m_u = m_d = 0.364$ GeV and $m_s = 0.565$ GeV.

We obtain G_S, G_V, κ, and m_s by the following procedure. We use the energies of the $\omega(1S)$ and $\omega(2S)$ states to fix $G_V = 12.46$ GeV^{-2} and $\kappa = 0.055$ GeV^2. We then use the mass of the $\phi(1020)$ to fix m_s at 0.565 GeV. Finally, we fix G_S at 12.46 GeV^{-2} by fitting the mass of the $K(495)$. The parameters G_K and G_{KA} are determined in our study of the K_1 and b_1 mesons and their specification will be described at a later point in our discussion. (The various parameters used in this work are listed in Table II for ease of reference.)

V. THE VECTOR NONET OF MESONS

The treatment of the vector nonet of mesons is simpler than that of the pseudoscalar nonet, since we may use ideal mixing for the ω and ϕ mesons. As noted earlier, the ω and

TABLE III. Vector mesons. Here $G_V=12.46$ GeV^{-2}, $m_u=0.364$ GeV, $m_s=0.565$ GeV, $\Lambda_3=0.622$ GeV, $\mu=0.01$ GeV, and $\kappa=0.055$ GeV^2.

Meson	Mass (Expt.) [MeV]	Mass (Theory) [MeV]	Spectroscopic character
$\omega(782)$[a]	781 ± 0.12	782	$1\ ^3S_1$
$\omega(1420)$[a]	1419 ± 31	1449	$2\ ^3S_1$
$\omega(1600)$	1649 ± 24	1591	$1\ ^3D_1$
		1766	$3\ ^3S_1$
		1828	$2\ ^3D_1$
$\phi(1020)$[a]	1019.413 ± 0.008	1015	$1\ ^3S_1$
$\phi(1680)$	1680 ± 20	1749	$2\ ^3S_1$
$K^*(892)$	891.59 ± 0.24	870	$1\ ^3S_1$
$K^*(1410)$	1412 ± 12	1590	$2\ ^3S_1$
$K^*(1680)$	1714 ± 20	1732	$1\ ^3D_1$
		1893	$3\ ^3S_1$

[a]These states are used to fix three parameters of the model: G_V, m_s, and κ.

ϕ mesons were discussed in Ref. [1]. We have repeated those calculations with the parameters used in this work: $G_V=12.46$ GeV^{-2}, $\kappa=0.055$ GeV^2, and $\mu=0.010$ GeV. The results are given in Table III and included in Fig. 1. We see that the 1^3D_1 state of the ω found in this work coincides in energy with the state designated as $^3D_1$ in Table 12.2 of Ref. [8].

We define a vector vertex *via* the equation

$$\bar{\Gamma}^{\mu}(P,k)=\hat{\gamma}^{\mu}-i\int\frac{d^4k'}{(2\pi)^4}[\gamma^{\rho}S(P/2+k')\bar{\Gamma}^{\mu}(P,k')\times S(-P/2+k')\gamma_{\rho}V^C(k-k')], \tag{5.1}$$

where $\hat{\gamma}^{\mu}=\gamma^{\mu}-P^{\mu}\not{P}/P^2$. The solution of this equation is described in Ref. [1]. We now define the tensor

$$-iJ_u^{\mu\nu}(P)=(-1)n_c\int\frac{d^4k}{(2\pi)^4}\mathrm{Tr}[iS_u(P/2+k)\times\bar{\Gamma}_u^{\mu}(P,k)iS_u(-P/2+k)\hat{\gamma}^{\nu}], \tag{5.2}$$

for the up quark and put

$$J_u^{\mu\nu}(P)=-\tilde{g}^{\mu\nu}(P)J_u^V(P^2), \tag{5.3}$$

with $\bar{g}^{\mu\nu}=g^{\mu\nu}-P^{\mu}P^{\nu}/P^2$. We then define $J_{\omega}(P^2)=2J_u^V(P^2)$. The mass of the ω and the masses of its radially-excited states are obtained by solving the equation

$$G_V^{-1}-J_{\omega}(P^2)=0. \tag{5.4}$$

The solution of this equation is exhibited in Fig. 3, where the horizontal line represents $G_V^{-1}=(12.46\ \mathrm{GeV}^{-2})^{-1}$. The mass values obtained from Eq. (5.4) are exhibited in Table III. It may be seen in Fig. 3 that the $2S$ state in the confining field is accompanied by the $1D$ state. (The splitting of these states is quite small, indicating that a very small tensor force is generated by our Lorentz-vector confinement model.) Further, the $2D$ state is found just above the $3S$ state, etc. Because of the short range of the NJL interaction, the $^3D_1$ states are hardly affected by that interaction.

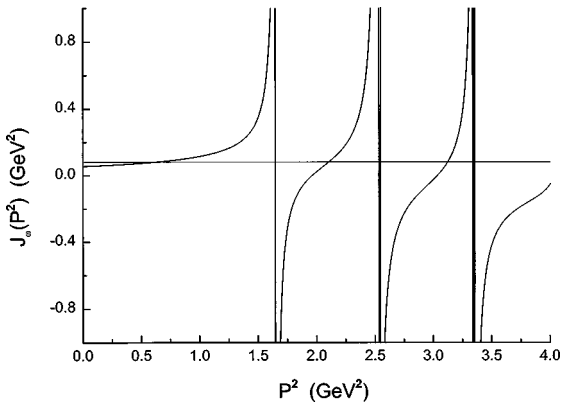

FIG. 3. The function $J_{\omega}(P^2)$ is shown. The horizontal line represents $G_V^{-1}=(12.46\ \mathrm{GeV}^{-2})^{-1}$. The intersections of that line and the curve representing $J_{\omega}(P^2)$ provide the solutions of the equation $G_V^{-1}-J_{\omega}(P^2)=0$.

The treatment of the ϕ meson is similar. We define $J_s^{\mu\nu}(P)$ in analogy to $J_u^{\mu\nu}(P)$ of Eq. (5.2) and then define

$$J_s^{\mu\nu}(P)=-\tilde{g}^{\mu\nu}(P)J_s^V(P^2) \tag{5.5}$$

and $J_{\phi}(P^2)=2J_s^V(P^2)$. Figure 4 shows the solution of the equation

$$G_V^{-1}-J_{\phi}(P^2)=0. \tag{5.6}$$

The mass values obtained in this manner are given in Table III.

We now need to generalize the results given in Ref. [1] to treat the case of differing quark and antiquark masses. We again consider $\hat{k}_{\mu}$ of Eq. (2.3) and recall the definition of $\hat{\gamma}^{\mu}$,

$$\hat{\gamma}^{\mu}=\gamma^{\mu}-P^{\mu}\not{P}/P^2. \tag{5.7}$$

We also define

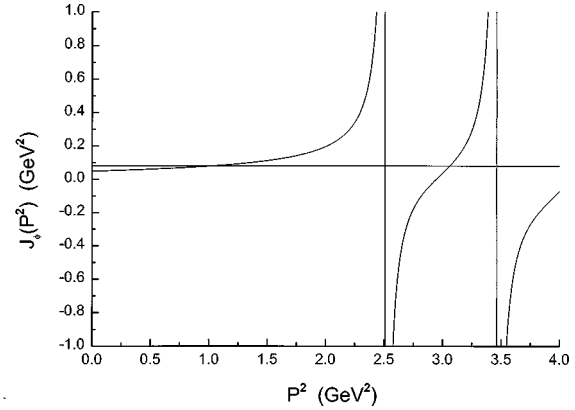

FIG. 4. The function $J_{\phi}(P^2)$ is shown. The horizontal line represents $G_V^{-1}=(12.46\ \mathrm{GeV}^{-2})^{-1}$. (See caption to Fig. 3.)

$$\gamma^{\mu}_{\perp,k} = \hat{\gamma}^{\mu} - \frac{\hat{k}^{\mu}\hat{\not{k}}}{\hat{k}^2}. \tag{5.8}$$

We see that $\hat{k}\cdot P = \gamma_{\perp\cdot k}\cdot P = \hat{k}\cdot\gamma_{\perp,k} = 0$. The set $\hat{k}^{\mu}$, $\gamma^{\mu}_{\perp,k}$ and P^{μ} is useful in setting up the equations for the vertex functions.

We now generalize Eq. (5.1) to read

$$\overline{\Gamma}^{\mu}_{ab}(P,k) = \hat{\gamma}^{\mu} - i\int \frac{d^4k'}{(2\pi)^4}[\gamma^{\rho}S_a(P/2+k')\overline{\Gamma}^{\mu}_{ab}(P,k') \times S_b(-P/2+k')\gamma_{\rho}]V^C(k-k'), \tag{5.9}$$

where we have introduced the possibility that m_a is unequal to m_b. We also define functions $\Gamma^{+-}_{1,ab}(P,k)$ and $\Gamma^{+-}_{2,ab}(P,k)$ in the frame where $\vec{P}=0$,

$$\Lambda^{(+)}_a(\vec{k})\overline{\Gamma}^{\mu}_{ab}(P,k)\Lambda^{(-)}_b(-\vec{k}) = \Gamma^{+-}_{1,ab}(P,k)\hat{k}^{\mu}\Lambda^{(+)}_a(\vec{k})\Lambda^{(-)}_b(-\vec{k}) + \Gamma^{+-}_{2,ab}(P,k)\Lambda^{(+)}_a(\vec{k})\gamma^{\mu}_{\perp,k}\Lambda^{(-1)}_b(-\vec{k}). \tag{5.10}$$

We introduce two additional functions

$$\gamma^{+-}_1(P,k) = \frac{-\vec{k}^2(m_a+m_b)}{2m_am_b}\Gamma^{+-}_{1,ab}(P,k) \tag{5.11}$$

and

$$\gamma^{+-}_2(P,k) = \Gamma^{+-}_{2,ab}(P,k). \tag{5.12}$$

A rather lengthy calculation yields coupled equations for γ^{+-}_1 and γ^{+-}_2. For $\alpha=1,2$ we have, with $k=|\vec{k}|$ and $k'=|\vec{k}'|$,

$$\gamma^{+-}_{\alpha}(P,k) = C_{\alpha} + \sum_{\alpha'=1,2}\int dk' \frac{t_{\alpha\alpha'}(k,k')\gamma^{+-}_{\alpha'}(P,k')}{P^0 - E_a(k') - E_b(k')}. \tag{5.13}$$

Here

$$C_1 = \frac{\vec{k}^2(m_a+m_b)^2}{2m_am_b[E_a(k)E_b(k)+\vec{k}^2-m_am_b]} \tag{5.14}$$

and

$$C_2 = 1. \tag{5.15}$$

Now we use the notation $E_a = E_a(\vec{k})$, $E'_a = E_a(\vec{k}')$, etc., to write

$$t_{11}(k,k') = \frac{kk'}{E'_aE'_b[E_aE_b+\vec{k}^2-m_am_b]}\left\{a_1(k,k')\left[(E'_aE'_b+\vec{k}'^2)(E_aE_b+\vec{k}^2) - m_am_b\left(E_aE_b+E'_aE'_b+\vec{k}^2+\vec{k}'^2-m_am_b - \frac{1}{2}E_aE'_b-\frac{1}{2}E'_aE_b\right) - \frac{1}{2}m_a^2E_bE'_b - \frac{1}{2}m_b^2E_aE'_a\right] + a_2(k,k')kk'\left[m_am_b+\frac{1}{2}m_a^2+\frac{1}{2}m_b^2\right]\right\}, \tag{5.16}$$

$$t_{12}(k,k') = \frac{\vec{k}^2\vec{k}'^2}{4m_am_bE'_aE'_b}\frac{[E'_aE'_b+\vec{k}'^2+m_am_b]}{[E_aE_b+\vec{k}^2-m_am_b]}[a_0(k,k')-a_2(k,k')], \tag{5.17}$$

$$t_{21}(k,k') = \frac{\vec{k}'^2m_am_b}{2E'_aE'_b}[a_0(k,k')-a_2(k,k'')], \tag{5.18}$$

and

$$t_{22}(k,k') = \frac{\vec{k}'^2}{4E'_aE'_b[E_aE_b+\vec{k}^2+m_am_b]}\{a_1(k,k')[E'_aE_b+E_aE'_b+E_aE'_a+E_bE'_b]+[a_0(k,k') + a_2(k,k')][(E_aE_b+\vec{k}^2)(E'_aE'_b+\vec{k}'^2)+m_am_b(E_aE_b+E'_aE'_b+\vec{k}^2+\vec{k}'^2+m_am_b)]\}. \tag{5.19}$$

In these equations

$$a_i(k,k') = \frac{1}{(2\pi)^3}\int_{-1}^{1}dx\,V^C(\vec{k}-\vec{k}')x^i, \tag{5.20}$$

with $x=\cos\theta$.

We also introduce the tensor

$$-iJ^{\mu\nu}_{ab}(P) = -2n_c\int\frac{d^4k}{(2\pi)^4}\mathrm{Tr}[iS_a(P/2+k)\overline{\Gamma}^{\mu}_{ab}(P,k) \times iS_b(-P/2+k)\hat{\gamma}^{\nu}] \tag{5.21}$$

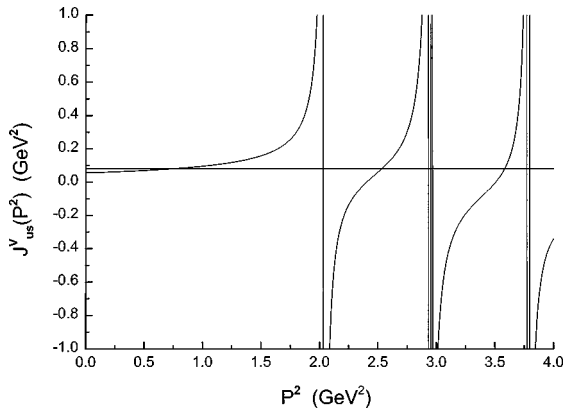

FIG. 5. The function $J^V_{us}(P^2)$ is shown. The vertical lines represent the energies of the bound states in the confining field. There is a $1\ ^3D_1$ slightly above the $2\ ^3S_1$ state and a $2\ ^3D_1$ state just above the $3\ ^3S_1$ state. The horizontal line represents $G_V^{-1}=(12.46\,\mathrm{GeV}^{-2})^{-1}$. The intersections of that line with the curve representing $J^V_{us}(P^2)$ yields the solutions of the equation $G_V^{-1}-J^V_{us}(P^2)=0$. (Note that the D states are hardly affected by the NJL interaction. For example, the $1\ ^3D_1$ state is found between the two vertical lines near $P^2=2.9\,\mathrm{GeV}^2$ when the NJL interaction is taken into account.) The energies of the K^* mesons found in this manner are given in Table III and shown in Fig. 1.

and put

$$J^{\mu\nu}_{ab}(P)=-\tilde{g}^{\mu\nu}(P)J^V_{ab}(P^2). \tag{5.22}$$

We obtain

$$J^V_{ab}(P^2)=\frac{-2n_c}{3}\int\frac{d^3k}{(2\pi)^3}\{-\vec{k}^2(m_a+m_b)\times\Gamma^{+-}_{1,ab}(P,k)+2(m_am_b+\vec{k}^2+E_aE_b)\times\Gamma_{2,ab}(P,k)\}\frac{1}{E_aE_b[P^0-E_a-E_b]}, \tag{5.23}$$

where the factor of 2 originates from the flavor trace.

We are now in a position to study the K^* mesons. In Fig. 5 we exhibit $J^V_{us}(P^2)$ and include a horizontal line representing $G_V^{-1}=(12.46\,\mathrm{GeV}^{-2})^{-1}$. In this manner we find states with the energies 0.870, 1.590, 1.732, and 1.893 GeV, where the third state is a D state—see Table III and Fig. 1. With no new parameters, we find that the energy of the $K^*(892)$ is fit rather well, while our state at 1.590 GeV is too high to provide a good fit the $K^*(1410)$. On the other hand, if the $K^*(1680)$ is indeed a $^3D_1$ state [8], we fit its energy quite well. (See Table 12.2 of Ref. [8].)

VI. THE SCALAR NONET

The scalar nonet of states is depicted in Fig. 6. We have studied the nonstrange isoscalar states, in the presence of singlet-octet mixing, in Ref. [11]. The situation is made complex by the very strong coupling of the scalar-isoscalar states to the $\pi\pi$ and $\tilde{K}K$ channels. (It has also been suggested that there is a 0^{++} glueball state with energy about 1.5 GeV,

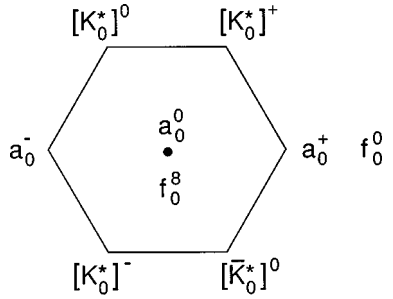

FIG. 6. States of the scalar nonet are shown.

which further complicates the picture.) Therefore, in the present work, we will concentrate on the properties of the K_0^* and a_0 mesons. To study the K_0^* states we again need to define the confining vertex and polarization functions for unequal masses of the quark and antiquark. We define $\overline{\Gamma}^S_{ab}(P,k)$ to be the solution of the equation

$$\overline{\Gamma}^S_{ab}(P,k)=1-i\int\frac{d^4k'}{(2\pi)^4}[\gamma^\rho S_a(P/2+k')\overline{\Gamma}^S_{ab}(P,k')\times S_b(-P/2+k')\gamma_\rho]V^C(k-k'). \tag{6.1}$$

We also introduce $\Gamma^{+-}_{S,ab}$ and $\Gamma^{-+}_{S,ab}$:

$$\Lambda^{(+)}_a(\vec{k})\overline{\Gamma}^S_{ab}(P,k)\Lambda^{(-)}_{ab}(-\vec{k})=\Gamma^{+-}_{S,ab}(P,k)\Lambda^{(+)}_a(\vec{k})\Lambda^{(-)}_b(-\vec{k}) \tag{6.2}$$

and

$$\Lambda^{(-)}_b(-\vec{k})\overline{\Gamma}^S_{ab}(P,k)\Lambda^{(+)}_a(\vec{k})=\Gamma^{-+}_{S,ab}(P,k)\Lambda^{(-)}_b(-\vec{k})\Lambda^{(+)}_a(\vec{k}). \tag{6.3}$$

We obtain the equation

$$\Gamma^{+-}_{S,ab}(P^0,k)=1-\frac{1}{(2\pi)^2}\int k'^2dk'\int_{-1}^{1}dx\,\frac{A_1(k,k',x)}{E_a(\vec{k}')E_b(\vec{k}')}\frac{1}{B(\vec{k})}\times\frac{\Gamma^{+-}_{S,ab}(P^0,k')V^C(\vec{k}-\vec{k}')}{P^0-E_a(\vec{k}')-E_b(\vec{k}')}, \tag{6.4}$$

with $x=\cos\theta$,

$$B(k)=[-E_a(\vec{k})E_b(\vec{k})-\vec{k}^2+m_am_b] \tag{6.5}$$

and

$$A_1(k,k',x)=\Big\{[E_a(\vec{k}')E_b(\vec{k}')+\vec{k}'^2][E_a(\vec{k})E_b(\vec{k})+\vec{k}^2]-m_am_b\Big[E_a(\vec{k})E_b(\vec{k})+E_a(\vec{k}')E_b(\vec{k}')+\vec{k}^2+\vec{k}'^2-m_am_b$$
$$-\frac{1}{2}E_a(\vec{k})E_b(\vec{k}')-\frac{1}{2}E_a(\vec{k}')E_b(\vec{k})\Big]-\frac{1}{2}m_a^2E_b(\vec{k}')E_b(\vec{k})-\frac{1}{2}m_b^2E_a(\vec{k})E_a(\vec{k}')+\vec{k}\cdot\vec{k}'\Big[m_am_b+\frac{1}{2}m_a^2+\frac{1}{2}m_b^2\Big]\Big\}. \tag{6.6}$$

Further,

$$\Gamma^{-+}_{S,ab}(P^0,k)=1-\frac{1}{(2\pi)^2}\int k'^2\,dk'\int_{-1}^{1}dx\,\frac{\tilde{A}_1(k,k',x)}{E_a(\vec{k}')E_b(\vec{k}')}\,\frac{1}{B(\vec{k})}\,\frac{\Gamma^{-+}_{S,ab}(P^0,k')V^C(\vec{k}-\vec{k}')}{P^0+E_a(\vec{k}')+E_b(\vec{k}')}, \tag{6.7}$$

where $\tilde{A}_1(k,k',x)$ is obtained from $A_1(k,k',x)$ by the replacements $E_a(\vec{k})\to -E_a(\vec{k})$ and $E_b(\vec{k})\to -E_b(\vec{k})$.

The result simplifies if $m_a=m_b$, such that

$$\Gamma^{+-}_S(P,k)=1+4\pi\int^{\Lambda_3}\frac{k'^2\,dk'}{(2\pi)^3}\,\frac{[(2k'^2k^2V_0(k,k'))+m^2kk'V_1(k,k')]}{k^2E^2(k')}\,\frac{\Gamma^{+-}_S(P,k')}{P^0-2E(\vec{k}')}, \tag{6.8}$$

where

$$V_i(k,k')=\frac{1}{2}\int_{-1}^{1}dx\,P_i(x)V^C(\vec{k}-\vec{k}'). \tag{6.9}$$

Here $P_i(x)$ is a Legendre function. We do not include $\Gamma^{-+}_{S,ab}(P,k)$ in our calculations, since the effect of including this function is small.

As a next step, we define

$$-iJ^S_{ab}(P^2)=(-2)n_c\int\frac{d^4k}{(2\pi)^4}\mathrm{Tr}[iS_a(P/2+k)\times\overline{\Gamma}^S_{ab}(P,k)iS_b(-P/2+k)], \tag{6.10}$$

where the factor of 2 again arises from the flavor trace. We obtain

$$J^S_{ab}(P^2)=-2n_c\int\frac{d^3k}{(2\pi)^3}\,\frac{[E_a(\vec{k})E_b(\vec{k})+\vec{k}^2-m_am_b]}{E_a(\vec{k})E_b(\vec{k})}\times\Big[\frac{\Gamma^{+-}_{S,ab}(P,k)}{P^0-E_a(\vec{k})-E_b(\vec{k})}-\frac{\Gamma^{-+}_{S,ab}(P,k)}{P^0+E_a(\vec{k})+E_b(\vec{k})}\Big]. \tag{6.11}$$

This result is quite simple, if $m_a=m_b$

$$J^S(P^2)=-4n_c\int\frac{d^3k}{(2\pi)^3}\,\frac{k^2}{E^2(\vec{k})}\times\Big[\frac{\Gamma^{+-}_S(P,k)}{P^0-2E(\vec{k})}-\frac{\Gamma^{-+}_S(P,k)}{P^0+2E(\vec{k})}\Big]. \tag{6.12}$$

We show $J^S_{ud}(P^2)$ for the equal mass case in Fig. 7 and include a line representing $G_S^{-1}=(12.46\,\mathrm{GeV}^{-2})^{-1}$. The intersection of that line with the line representing the function $J^S_{ud}(P^2)$ determines the energy of the states $a_0(1S)$, $a_0(2S)$, and $a_0(3S)$. These energies are given in Table IV.

In Fig. 8 we show the function $J^S_{us}(P^2)$ and a horizontal line representing G_S^{-1}. We find K_0^* states at 1.412 GeV, 1.738 GeV, and 1.999 GeV. (See Table IV.) There are two states given in the data tables [8], the $K_0^*(1430)$ and $K_0^*(1950)$. We find a $2\ ^3P_0$ state between these states, suggesting that the $K_0^*(1950)$ may be a $3\ ^3P_0$ state. [Note that we fit the mass of the $K_0^*(1430)$ without the introduction of any additional parameters.]

VII. AXIAL-VECTOR NONETS

In Fig. 9 we exhibit the $^3P_1$ and $^1P_1$ axial-vector nonets, as described in the constituent quark model. When using the NJL model in relativistic calculations, it is somewhat more

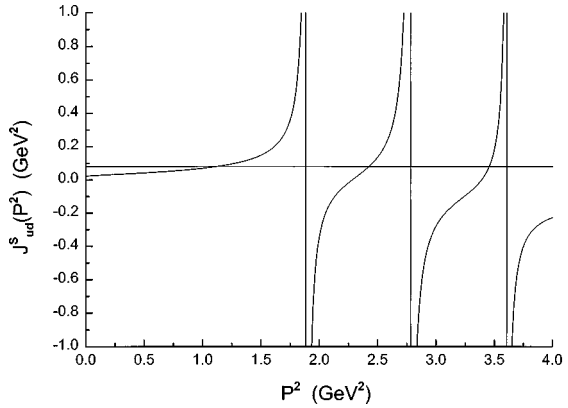

FIG. 7. The function $J^S_{ud}(P^2)$ is shown. The horizontal line represents $G_S^{-1}=(12.46\,\mathrm{GeV}^{-2})^{-1}$. (See Table IV for masses of the a_0 mesons.)

TABLE IV. Mass values of scalar mesons. See Table II for a list of parameters. No parameters are varied in these fits to the data.

Meson	Mass (Expt.) [MeV]	Mass (Theory) [MeV]	Spectroscopic character
$K_0^*(1430)$	$1429\pm4\pm5$	1416	$1\ ^3P_0$
		1738	$2\ ^3P_0$
$K_0^*(1950)$[a]	$1945\pm10\pm20$	1999	$3\ ^3P_0$
$a_0(980)$	983.5 ± 0.9	1063	$1\ ^3P_0$
$a_0(1450)$[a]	1450 ± 50	1556	$2\ ^3P_0$
		1857	$3\ ^3P_0$

[a]Needs confirmation.

convenient to characterize the nonets by the NJL interaction for that nonet. For example, we will use the NJL interaction that gives rise to the vertices $\gamma^\mu\gamma_5$ to calculate the properties of what is usually called the $^3P_1$ nonet. At a later point in the discussion, we will introduce another interaction that we use to perform dynamical calculations for what is the $^1P_1$ nonet in the constituent quark model. Since, the vertex $\gamma^\mu\gamma_5$ acts to a small degree in $^1P_1$ states, we do not have an exact separation into $^3P_1$ and $^1P_1$ states. However, our procedure is particularly convenient when we perform fully relativistic calculations using the NJL model. This aspect of our calculations will become more apparent as we continue our presentation. Although the axial current is not conserved, we need not consider vertices that depend upon P^μ when working in the meson rest frame. Thus, we consider the vertex associated with the matrix $\hat{\gamma}^\mu\gamma_5$ and define $\Gamma^{+-}_{A,1}(P,k)$ and $\Gamma^{+-}_{A,2}(P,k)$, such that

$$\begin{aligned}\Lambda_a^{(+)}(\vec{k})\bar{\Gamma}^\mu_{A,ab}(P,k)\Lambda_b^{(-)}(-\vec{k})&\\ =\Gamma^{+-}_{A,1,ab}(P,k)\hat{k}^\mu\Lambda_a^{(+)}(\vec{k})\gamma_5\Lambda_b^{(-)}(-\vec{k})&\\ +\Gamma^{+-}_{A,2,ab}(P,k)\Lambda_a^{(+)}(\vec{k})\gamma^\mu_{\perp,k}\gamma_5\Lambda_b^{(-)}(-\vec{k}).&\quad(7.1)\end{aligned}$$

We note that $\bar{\Gamma}^\mu_A(P,k)$ satisfies the equation

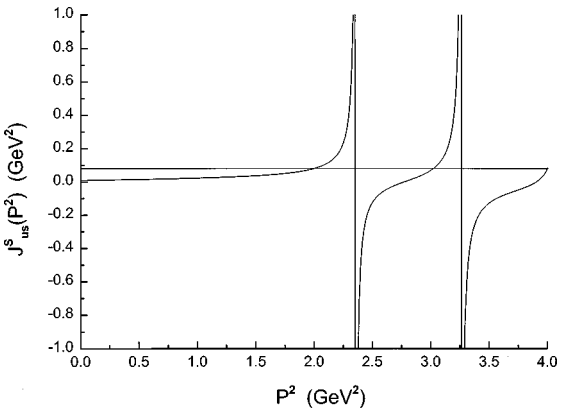

FIG. 8. The function $J^S_{us}(P^2)$ is shown. The horizontal line represents $G_S^{-1}=(12.46\,\mathrm{GeV}^{-2})^{-1}$. (See Table IV for masses of the K_0^* mesons.)

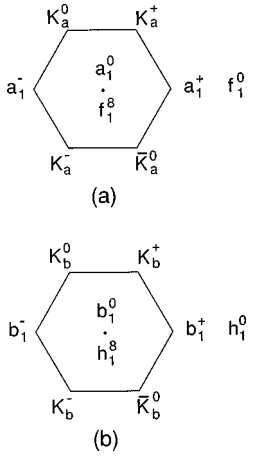

FIG. 9. The $^3P_1$ and $^1P_1$ nonets of axial-vector mesons are shown.

$$\begin{aligned}\bar{\Gamma}^\mu_A(P,k)=\hat{\gamma}^\mu\gamma_5-i\int\frac{d^4k'}{(2\pi)^4}[\gamma^\rho S_a(P/2+k')\bar{\Gamma}^\mu_A(P,k')&\\ \times S_b(-P/2+k')\gamma_\rho]V^C(k-k').&\quad(7.2)\end{aligned}$$

For $\alpha=1,2$, we have

$$\Gamma^{+-}_{A,\alpha}(P,k)=D_\alpha+\sum_{\alpha'=1,2}\int dk'\frac{t_{\alpha\alpha'}(k,k')\Gamma^{+-}_{A,\alpha'}(P,k')}{P^0-E_a(k')-E_b(k')},\quad(7.3)$$

with

$$D_1=\frac{m_b-m_a}{E_aE_b+\vec{k}^2+m_am_b}\quad(7.4)$$

and

$$D_2=1.\quad(7.5)$$

Here we have put $E_a=E_a(\vec{k})$, $E'_a=E'_a(\vec{k})$, etc. We have

$$\begin{aligned}t_{11}(k,k')=\frac{\vec{k}'^3}{\vec{k}E'_aE'_b[E_aE_b+\vec{k}^2+m_am_b]}&\\ \times\Bigg\{a_1(k,k')\Bigg[(E'_aE'_b+\vec{k}'^2)(E_aE_b+\vec{k}^2)&\\ +m_am_b\Bigg(E_aE_b+E'_aE'_b+\vec{k}^2+\vec{k}'^2+m_am_b&\\ -\frac{1}{2}E_aE'_b-\frac{1}{2}E'_aE_b\Bigg)-\frac{1}{2}m_a^2E_bE'_b-\frac{1}{2}m_b^2E_aE'_a\Bigg]&\\ +a_2(k,k')kk'\Bigg[-m_am_b+\frac{1}{2}m_a^2+\frac{1}{2}m_b^2\Bigg]\Bigg\},&\quad(7.6)\end{aligned}$$

$$t_{12}(k,k')=\frac{-\vec{k}'^2(m_a-m_b)}{2E'_aE'_b}\,\frac{[E'_aE'_b+\vec{k}'^2-m_am_b]}{[E_aE_b+\vec{k}^2+m_am_b]}\times[a_0(k,k')-a_2(k,k')], \tag{7.7}$$

$$t_{21}(k,k')=\frac{\vec{k}'^4(m_b-m_a)}{4E'_aE'_b}[a_0(k,k')-a_2(k,k')], \tag{7.8}$$

and

$$t_{22}(k,k')=\frac{\vec{k}'^2}{4E'_aE'_b[E_aE_b+\vec{k}^2-m_am_b]}\{a_1(k,k')\times[E'_aE_b+E_aE'_b+E_aE'_a+E_bE'_b]+[a_0(k,k')+a_2(k,k')][(E_aE_b+\vec{k}^2)(E'_aE'_b+\vec{k}'^2)-m_am_b(E_aE_b+E'_aE'_b+\vec{k}^2+\vec{k}'^2-m_am_b)]\}. \tag{7.9}$$

Note that when $m_a=m_b$, the inhomogeneous term $D_1=0$. That feature has its origin in the fact that we can write

$$\hat{\gamma}^\mu\gamma_5=\gamma^\mu_{\perp,k}\gamma_5+\frac{\hat{k}^\mu\hat{k}}{\hat{k}^2}\gamma_5, \tag{7.10}$$

and note that $\overline{u}(\vec{k},s')\hat{k}v(-\vec{k},-s)=0$ in the equal-mass case. The remaining matrix, $\gamma^\mu_{\perp,k}\gamma_5$ governs the interaction in $^3P_1$ states.

We will also need to define

$$-iJ^{\mu\nu}_{A,ab}(P^2)=(-2)n_c\int\frac{d^4k}{(2\pi)^4}\times\mathrm{Tr}[iS_a(P/2+k)\overline{\Gamma}^\mu_{A,ab}(P,k)\times iS_b(-P/2+k)\hat{\gamma}^\nu\gamma_5]. \tag{7.11}$$

We write

$$J^{\mu\nu}_{A,ab}(P)=-\tilde{g}^{\mu\nu}(P)J^A_{ab}(P^2), \tag{7.12}$$

with $\tilde{g}^{\mu\nu}(P)=g^{\mu\nu}-P^\mu P^\nu/P^2$, and find that

$$J^A_{ab}(P^2)=\frac{-2n_c}{3}\int\frac{d^3k}{(2\pi)^3}\{-\vec{k}^2(m_a-m_b)\Gamma^{+-}_{A,1,ab}(P,k)+2(-m_am_b+\vec{k}^2+E_aE_b)\Gamma^{+-}_{A,2,ab}(P,k)\}\times\frac{1}{E_aE_b[P^0-E_a-E_b]}. \tag{7.13}$$

Using this formalism, we obtained the values of $J^A_{us}(P^2)$ given in Fig. 10. We interpret the figure as follows. The pair of vertical lines at about 2.5 GeV^2 and 3.4 GeV^2 represent the energies of the 1 $^3P_1$ and 1 $^1P_1$ states and the 2 $^3P_1$ and 2 $^1P_1$ states, respectively, in the absence of the NJL interaction. It is then found that the 1 $^3P_1$ moves down to 1.41 GeV and the 2 $^3P_1$ state moves down to 1.75 GeV when the NJL interaction is considered. On the other hand, the 1 $^1P_1$ and 2 $^1P_1$ states move hardly at all from their original position. (One may say that the two $^1P_1$ states are ''trapped'' between the pairs of vertical lines.) This behavior follows from the structure of the NJL model, since there is no interaction term that acts on the $^1P_1$ states, except for the second term in Eq. (7.10), which yields quite small effects. Since it is known that there is significant $^3P_1$ and $^1P_1$ mixing for the strange axial-vector mesons [12], we need to modify the NJL Lagrangian to deal with this problem. We take up that matter in Sec. VIII.

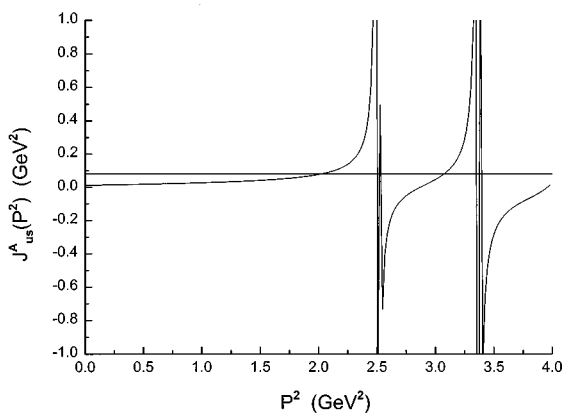

FIG. 10. The function $J^A_{us}(P^2)$ is shown. The first pair of vertical lines at about 2.5 GeV^2 indicate the energies of the 1 $^3P_1$ and 1 $^1P_1$ states in the confining field with the 1 $^3P_1$ state having a lower energy. The second pair of vertical lines show the positions of the 2 $^3P_1$ and 2 $^1P_1$ states in the confining field. The horizontal line represents $G_V^{-1}=(12.46\ \mathrm{GeV}^{-2})^{-1}$. Note that only the $^3P_1$ states move down in energy to any significant degree, when the NJL interaction is taken into account.

For the equal mass case, the $^3P_1$ and $^1P_1$ states are uncoupled. Therefore, we can use the equation for $\Gamma^{+-}_{A,2}(P,k)$ and the values of $J^A(P^2)$ for the equal mass case, to find the energies of the a_1 meson and its radially-excited states. We find a state at 1239 MeV which can be identified as the $a_1(1260)$. (That state is assigned an energy of 1230 ± 40 MeV in the data tables [8].) The radial excitations of the a_1, 2 $^3P_1$ and 3 $^3P_1$ states, are at 1600 and 1895 MeV, respectively. (See Fig. 1 and Table V.) Note that this analysis is quite consistent with the fact that the $b_1(1235)$, which is assigned an energy of 1231 ± 10 MeV in the data tables [8], is essentially degenerate with the $a_1(1260)$. [Recall that the $a_1(1260)$ has an energy of 1230 ± 40 MeV in the data tables

TABLE V. Mass values of the a_1 mesons.

Meson	Mass (Expt.) [MeV]	Mass (Theory) [MeV]	Spectroscopic character
$a_1(1260)$	1230 ± 40	1220	1 $^3P_1$
		1600	2 $^3P_1$
		1895	3 $^3P_1$

and 1239 MeV in our calculations.] This aforementioned degeneracy appears in the NJL model, since there is no $^3P_1$-$^1P_1$ mixing for $m_a=m_b$, which is the case for the $^3P_1$ a_1 mesons and the $^1P_1$ b_1 mesons.

VIII. AN EXTENDED NJL MODEL FOR THE STUDY OF $^3P_1$-$^1P_1$ MIXING

The NJL model has only a very weak interaction in $^1P_1$ states, as may be seen in Fig. 10. Whatever interaction exists arises from the small coupling of the $^1P_1$ states to the $^3P_1$ states that appears in the coupled equations for $\Gamma^{+-}_{A,1,ab}$ and $\Gamma^{+-}_{A,2,ab}$ given in the last section. (We recall that the coupling term and D_1 vanish when $m_a=m_b$.)

Since it is believed that the $^3P_1$ and $^1P_1$ states are mixed with a mixing angle of about 45° in the case of the strange axial-vector mesons [12], we wish to extend the NJL model to treat such coupling. The natural choice for such a generalization is an interaction Lagrangian that preserves the chiral symmetry of the original Lagrangian:

$$\mathcal{L}_{\rm int}=\frac{G_K}{4M^2}\sum_{i=0}^{8}[(i\bar{q}\lambda^i\partial_\mu q)(-i\partial_\mu\bar{q}\lambda^i q) -(\bar{q}\lambda^i\gamma_5 i\partial_\mu q)(-i\partial_\mu\bar{q}\lambda^i\gamma_5 q)]. \tag{8.1}$$

Such an interaction actually appears in a natural fashion, if we consider a gradient expansion of the effective quark interaction. (One can envision a series of terms which have varying numbers of gradients.) In Eq. (8.1) we have inserted a factor of $1/M^2$ so that G_k has the same dimension as G_S and G_V. For our convenience, we take $M=1.0$ GeV, although any other value will do.

It is now natural to consider an additional vertex equation with an inhomogeneous term $\hat{k}^\mu\gamma_5$. Thus, we define

$$\bar{\Gamma}^\mu_{B,ab}(P,k)=\hat{k}^\mu\gamma_5-i\int\frac{d^4k'}{(2\pi)^4}[\gamma^\rho S_a(P/2+k') \times\bar{\Gamma}^\mu_{B,ab}(P,k')S_b(-P/2+k')\gamma_\rho] \times V^C(k-k') \tag{8.2}$$

and also write

$$\Lambda^{(+)}_a(\vec{k})\bar{\Gamma}^\mu_{B,ab}(P,k)\Lambda^{(-)}_b(-\vec{k}) =\Gamma^{+-}_{B,1,ab}(P,k)\hat{k}^\mu\Lambda^{(+)}_a(\vec{k})\gamma_5\Lambda^{(-)}_b(-\vec{k}) +\Gamma^{+-}_{B,2,ab}(P,k)\Lambda^{(+)}_a(\vec{k})\gamma^\mu_{\perp,k}\gamma_5\Lambda^{(-)}_b(-\vec{k}). \tag{8.3}$$

We obtain the equation

$$\Gamma^{+-}_{B,\alpha,ab}(P,k) =E_\alpha+\sum_{\alpha'=1,2}\int dk'\frac{t_{\alpha\alpha'}(k,k')\Gamma^{+-}_{B,\alpha',ab}(P,k')}{P^0-E_a(k')-E_b(k')}, \tag{8.4}$$

with $E_1=1$ and $E_2=0$. This equation is the same as that given previously for $\bar{\Gamma}^{+-}_A$ except that D_1 is replaced by E_1 and D_2 is replaced by E_2. Note that, since the homogeneous equations for $\bar{\Gamma}^\mu_A$ and $\bar{\Gamma}^\mu_B$ are the same, these functions will have singularities at the same energies. These energies represent the energies of the bound states in the confining field set up by $V^C(\vec{k}-\vec{k}')$.

We now define four polarization functions. First, we introduce

$$-iJ^{\mu\nu}_{11}(P^2)_{ab}=(-2)n_c\int\frac{d^4k}{(2\pi)^4} \times{\rm Tr}[iS_a(P/2+k)\bar{\Gamma}^\mu_{B,ab}(P,k) \times iS_b(-P/2+k)\hat{k}^\nu\gamma_5], \tag{8.5}$$

and put

$$J^{\mu\nu}_{11}(P)_{ab}=-\tilde{g}^{\mu\nu}(P)J^A_{11}(P^2). \tag{8.6}$$

We find that $J^A_{11}(P^2)$ does not depend upon $\Gamma^{+-}_{B,2,ab}$,

$$J^A_{11}(P^2)=-\frac{2}{3}n_c\int\frac{d^3k}{(2\pi)^3}\frac{\vec{k}^2}{E_a(\vec{k})E_b(\vec{k})} \times\frac{[E_a(\vec{k})E_b(\vec{k})+\vec{k}^2+m_am_b]}{P^0-E_a(\vec{k})-E_b(\vec{k})}\Gamma^{+-}_{B,1,ab}(P,k). \tag{8.7}$$

We also define

$$-iJ^{\mu\nu}_{12}(P^2)_{ab}=(-2)n_c\int\frac{d^4k}{(2\pi)^4} \times{\rm Tr}[iS_a(P/2+k)\bar{\Gamma}^\mu_{B,ab}(P,k) \times iS_b(-P/2+k)\hat{\gamma}^\nu\gamma_5]. \tag{8.8}$$

With

$$J^{\mu\nu}_{12}(P)_{ab}=-\tilde{g}^{\mu\nu}(P)J^A_{12}(P^2), \tag{8.9}$$

we obtain

$$J^A_{12}(P^2)=\frac{-2n_c}{3}\int\frac{d^3k}{(2\pi)^3}\{-\vec{k}^2(m_a-m_b)\Gamma^{+-}_{B,1,ab}(P,k) +2(-m_am_b+\vec{k}^2+E_aE_b)\Gamma^{+-}_{B,2,ab}(P,k)\} \times\frac{1}{E_aE_b[P^0-E_a-E_b]}, \tag{8.10}$$

which is of the form of Eq. (7.13) with the replacement $\Gamma^{+-}_{A,1,ab}(P,k)\to\Gamma^{+-}_{B,1,ab}(P,k)$ and $\Gamma^{+-}_{A,2,ab}(P,k)\to\Gamma^{+-}_{B,2,ab}(P,k)$.

We also note that $J^A_{21}(P^2)=J^A_{12}(P^2)$, where the definition of $J^A_{21}(P^2)$ is straightforward. The polarization function

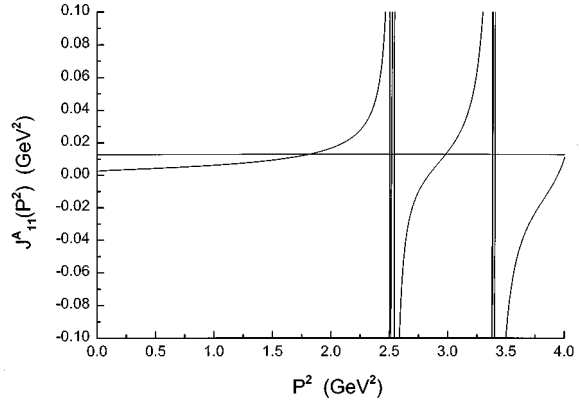

FIG. 11. The function $J^A_{11}(P^2)/M^2$ is shown. The intersection of that curve with the horizontal line representing $G_K^{-1} = (78.13\,\mathrm{GeV}^{-2})^{-1}$ yields the (uncoupled) spectrum shown in Fig. 14(a). (Here $M = 1.0$ GeV.)

$J^A_{22}(P^2)$ may be identified with our result for $J^A_{ab}(P^2)$ given in Eq. (7.13). We also see that J^A_{11}, J^A_{12}, and J^A_{22} will have singularities at the same values of P^2. Values of $J^A_{11}(P^2)$ are given in Fig. 11 and $J^A_{12}(P^2)$ is shown in Fig. 12.

We now define a T matrix for the coupled $^3P_1$-$^1P_1$ system, which we organize in a matrix form,

$$\hat{T} = (\hat{k}_\mu \gamma_5, \hat{\gamma}_\mu \gamma_5) \begin{pmatrix} T^{\mu\nu}_{11}(P) & T^{\mu\nu}_{12}(P) \\ T^{\mu\nu}_{21}(P) & T^{\mu\nu}_{22}(P) \end{pmatrix} \begin{pmatrix} \hat{k}_\nu \gamma_5 \\ \hat{\gamma}_\nu \gamma_5 \end{pmatrix}, \tag{8.11}$$

and put $T^{\mu\nu}_{11}(P) = -g^{\mu\nu} T_{11}(P^2)$, $T^{\mu\nu}_{12}(P) = -g^{\mu\nu} T_{12}(P^2)$, $T^{\mu\nu}_{21}(P) = -g^{\mu\nu} T_{21}(P^2)$, and $T^{\mu\nu}_{22}(P) = -g^{\mu\nu} T_{22}(P^2)$.

We introduce the matrices

$$G = \begin{pmatrix} -G_K & 0 \\ 0 & -G_V \end{pmatrix}, \tag{8.12}$$

$$J(P^2) = \begin{pmatrix} J^A_{11}(P^2)/M^2 & J^A_{12}(P^2)/M \\ J^A_{21}(P^2)/M & J^A_{22}(P^2) \end{pmatrix}, \tag{8.13}$$

and

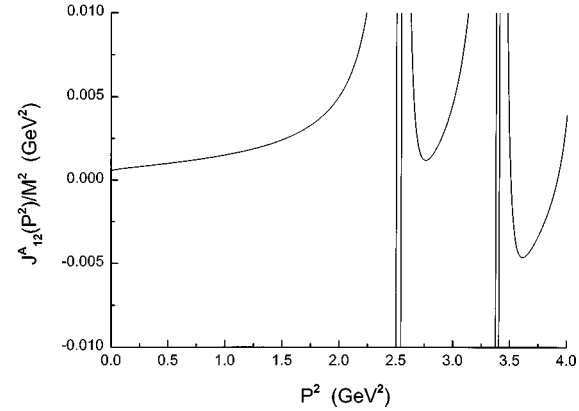

FIG. 12. The function $J^A_{12}(P^2)/M$ is shown. (Here $M = 1.0$ GeV.)

$$T(P^2) = \begin{pmatrix} T_{11}(P^2) & T_{12}(P^2) \\ T_{21}(P^2) & T_{22}(P^2) \end{pmatrix}. \tag{8.14}$$

We then have the matrix equation

$$T(P^2) = G - GJ(P^2)T(P^2), \tag{8.15}$$

or

$$[1 + GJ(P^2)]T(P^2) = G, \tag{8.16}$$

so that $T(P^2) = D^{-1}(P^2)G$, with

$$D(P^2) = \begin{pmatrix} 1 - G_K J^A_{11}(P^2)/M^2 & -G_K J^A_{12}(P^2)/M \\ -G_V J^A_{12}(P^2)/M & 1 - G_V J^A_{22}(P^2) \end{pmatrix}. \tag{8.17}$$

Thus

$$T_{11}(P^2) = -\frac{G_K[1 - G_V J^A_{22}(P^2)]}{\det D(P^2)}, \tag{8.18}$$

$$T_{12}(P^2) = \frac{-G_V G_K J^A_{12}(P^2)/M}{\det D(P^2)}, \tag{8.19}$$

and

$$T_{22}(P^2) = \frac{-G_V[1 - G_K J^A_{11}(P^2)/M^2]}{\det D(P^2)}, \tag{8.20}$$

where

$$\det D(P^2) = [1 - G_K J^A_{11}(P^2)/M^2][1 - G_V J^A_{22}(P^2)/M] - G_K G_V [J^A_{12}(P^2)/M]^2. \tag{8.21}$$

We may obtain the spectrum of the coupled system from the equation

$$\det D(P^2) = 0. \tag{8.22}$$

Alternately, we may bring the T matrix to diagonal form at each value of P^2, such that

$$M(\phi)T(P^2)M^{-1}(\phi) = \begin{pmatrix} T_1(P^2) & 0 \\ 0 & T_2(P^2) \end{pmatrix}, \tag{8.23}$$

with

$$M(\phi) = \begin{pmatrix} \cos\phi & -\sin\phi \\ \sin\phi & \cos\phi \end{pmatrix}, \tag{8.24}$$

where ϕ is a function of P^2. Resonances or bound states appear as singularities of $T_1(P^2)$ and $T_2(P^2)$.

We may first consider the case where $J^A_{12}(P^2) = 0$. We determine the parameter G_K by fitting the energy of the $b_1(1235)$ meson by solving the equation

$$G_K^{-1} - J^A_{11,ud}(P^2) = 0, \tag{8.25}$$

where $J^A_{11,ud}(P^2)$ is $J^A_{11}(P^2)$ calculated in the equal-mass case with $m_a = m_b = 0.364$ GeV. (See Fig. 13.) Here we are

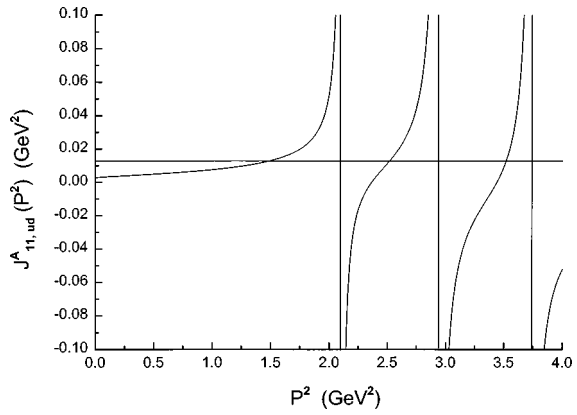

FIG. 13. The function $J^A_{11,ud}(P^2)$ is shown. Here $m_a = m_b = 0.364$ GeV. The horizontal line represents $G_K^{-1} = (78.13\ \mathrm{GeV}^{-2})^{-1}$. The intersection of that line with curve representing $J^A_{11,ud}(P^2)$ yields the mass values for the b_1 mesons given in Table VI. Here we assume ideal mixing.

assuming that we have ideal mixing for the b_1 mesons. We find that $G_K = 78.13\ \mathrm{GeV}^{-2}$ yields the mass values given in Table VI.

We now consider the $^3P_1$ and $^1P_1$ K_1 mesons in the uncoupled case. The mass values obtained from the solution of the equations

$$G_K^{-1} - J^A_{11}(P^2) = 0 \tag{8.26}$$

and

$$G_V^{-1} - J^A_{22}(P^2) = 0 \tag{8.27}$$

are given in Figs. 14(a) and 14(b), respectively. (Recall that J^A_{11} and J^A_{22} are defined with $m_a = m_u$ and $m_b = m_s$ in this case.)

We now proceed to discuss $^3P_1$-$^1P_1$ mixing for the strange axial-vector mesons. Our first observation is that $J^A_{12}(P^2)$ is quite small and leads to relatively little mixing. We note that if we do not use the energy of the $b_1(1235)$ to fix G_K, we may put $G_K = 93.0\ \mathrm{GeV}^{-2}$ and provide a rather good fit to the masses of the K_1 mesons. However, we continue to maintain $G_K = 78.13\ \mathrm{GeV}^{-2}$ and consider another model for $^3P_1$-$^1P_1$ mixing. We replace the matrix G of Eq. (8.12) by

$$G = -\begin{pmatrix} G_K & G_{KA} \\ G_{KA} & G_V \end{pmatrix}. \tag{8.28}$$

TABLE VI. Mass values for the b_1 mesons under the assumption of ideal mixing. [See Fig. 14(d).] Here $m_a = m_b = 0.364$ GeV.

Meson	Mass (Expt.) [MeV]	Mass (Theory) [MeV]	Spectroscopic character
$b_1(1235)$	1231 ± 10	1230[a]	$1\ ^1P_1$
		1587	$2\ ^1P_1$
		1876	$3\ ^1P_1$

[a]This state is used to fix $G_K = 78.13\ \mathrm{GeV}^{-2}$.

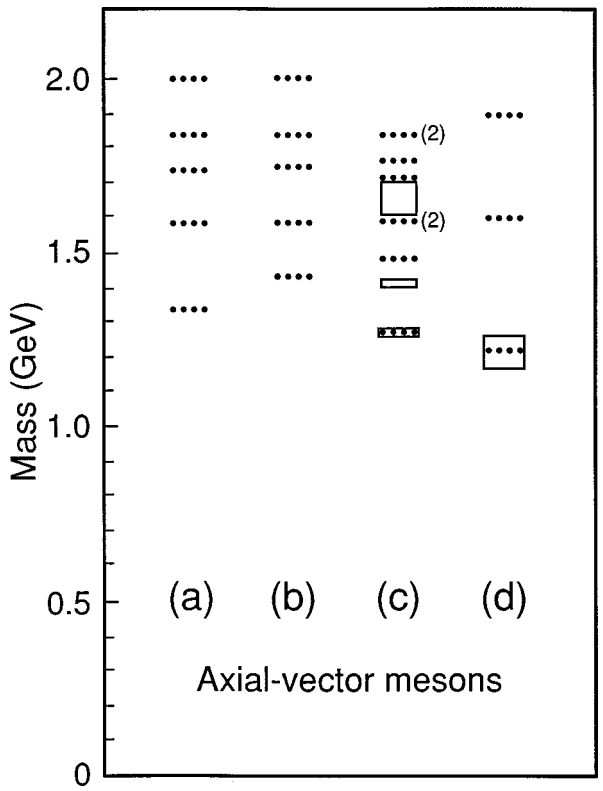

FIG. 14. (a) The mass values obtained from the solution of the equation $G_K^{-1} - J^A_{11}(P^2) = 0$ are represented by dotted lines. Here $G_K = 78.13\ \mathrm{GeV}^{-2}$. We find states with mass values of 1.35, 1.59, 1.73, 1.84, and 2.00 GeV. (b) The mass values obtained from the solution of the equation $G_V^{-1} - J^A_{22}(P^2) = 0$ are shown as dotted lines. (Here $G_V = 12.46\ \mathrm{GeV}^{-2}$.) We find states with mass values of 1.43, 1.59, 1.75, 1.84, and 2.01 GeV. Note that $J^A_{22}(P^2)$ is the same as $J^A_{us}(P^2)$ shown in Fig. 10. (c) The states of the K_1 meson, calculated with $G_K = 78.13\ \mathrm{GeV}^{-2}$ and $G_{KA} = 8.00\ \mathrm{GeV}^{-2}$, are compared to the data. Here we include the mixing due to the polarization functions $J^A_{12}(P^2)$ and $J^A_{21}(P^2)$, as well as that due to the direct coupling parametrized by G_{KA}. (See Table VII.) (d) Masses of the b_1 mesons. (See Table VI.)

It is clear that G_{KA} couples the $^3P_1$ and $^1P_1$ channels directly. (The equations for the T matrix have to be modified appropriately.) We find that $G_{KA} = 8.00\ \mathrm{GeV}^{-2}$ gives rise to the K_1 energies given in Table VII and shown in Fig. 14(c).

We now turn to a discussion of the mixing angle, coupling constant, and form factors, as defined in our covariant formulation. Near a singularity of $T_1(P^2)$ at $P^2 = m_1^2$ we may define

$$\langle k' | \hat{T}(P^2) | k \rangle = -F^A_\mu(k') \frac{\tilde{g}^{\mu\nu}}{P^2 - m_1^2} F^A_\nu(k), \tag{8.29}$$

with

$$F^\mu_A(k) = g_1 \left[\frac{\hat{k}^\mu \gamma_5}{M} \cos\phi - \hat{\gamma}^\mu \gamma_5 \sin\phi \right]. \tag{8.30}$$

In Eq. (8.30), g_1 is a coupling constant.

TABLE VII. Theoretical and experimental values of the masses of the axial-vector K_1 mesons. See Eqs. (8.30) and (8.31) for definitions of the coupling constant and mixing angle.

Meson	Mass (Expt.) [MeV]	Mass (Theory) [MeV]	Mixing angle ϕ	g_1
$K_1(1270)$	1275 ± 10	1274[a]	$-15.2°$	8.60
$K_1(1400)$	1402 ± 7	1483	40.9°	3.13
$K_1(1650)$	1650 ± 50	1594[b]		
		1722		
		1722		
		1838[b]		

[a]Fit by the choice $G_{KA}=8.0\,\mathrm{GeV}^{-2}$, when $M=1.0$ GeV. [See Eq. (8.28).]

[b]These are doublets weakly coupled to quarks.

We may also modify the vertex form factor, $F_A^\mu(k)$, to include the effects of confinement using the methods developed in Ref. [3]. [With that procedure, we are able to show that $\hat{T}(P^2)$ is represented by bound states only, if the potential V^C is absolutely confining. Note that we have already modified the vacuum polarization integrals to include confinement effects.] To include confinement effects in the numerator of the T matrix of Eq. (8.29), we replace Eq. (8.30) by [3]

$$\tilde{F}^\mu(P,k)=g_1\left[\frac{\overline{\Gamma}_B^\mu(P,k)}{M}\cos\phi-\overline{\Gamma}_A^\mu(P,k)\sin\phi\right], \tag{8.31}$$

where $P^2=m_1^2$. The mixing angle, ϕ, is given in Table VII for the first two states of Fig. 14(c). However, that angle is particular to our method of calculation and does not correspond to the angle introduced to describe mixing of $^3P_1$ and $^1P_1$ octets in Ref. [12], for example.

One interesting feature of the $K_1(1270)$ and the $K_1(1400)$ mesons is that they have differing predominant decay channels. For example, the decay width for $K_1(1400)\to K^*+\pi$ is much larger than the width for $K_1(1400)\to K+\rho$. On the other hand, the $K_1(1270)$ decays predominantly to $K+\rho$, with weaker decay to the $K^*+\pi$ channel. This feature suggests approximately equal mixtures of $^3P_1$ and $^1P_1$ states in these K_1 mesons, as discussed by Suzuki, for example [12], where a single mixing angle is used for the $K_1(1270)$ and $K_1(1400)$. However, in the case of composite mesons, the mixing angle is P^2-dependent, as is the case in our work. [To use the formalism used in Ref. [12], one must assume that the $K_1(1270)$ and $K_1(1400)$ are elementary particles.]

Finally, we calculate the mass values for the $s\overline{s}$ states of the f_1 and h_1 mesons, under the assumption of ideal mixing. For the f_1 we consider the equation

$$G_V^{-1}-J^A_{22,ss}(P^2)=0, \tag{8.32}$$

where $J^A_{22,ss}(P^2)$ has $m_a=m_b=m_s$. For the h_1 meson, we solve

$$G_K^{-1}-J^A_{11,ss}(P^2)=0, \tag{8.33}$$

TABLE VIII. Mass values of $s\overline{s}$ axial-vector mesons in the case of ideal mixing. Here $m_a=m_b=0.565$ GeV.

Meson	Mass (Theory) [MeV]	Spectroscopic character
f_1	1600	$1\ ^3P_1$
	1902	$2\ ^3P_1$
h_1	1468	$1\ ^1P_1$
	1871	$2\ ^1P_1$

where $J^A_{11,ss}(P^2)$ also has $m_a=m_b=m_s$. Mass values obtained in this manner are given in Table VIII. It is uncertain as to whether ideal mixing is appropriate for the f_1 and h_1 mesons and an analysis similar to that made for the η-η' system, with a reduced attraction in singlet states, may be most appropriate. (Recall that in our study of η-η' mixing, we used G_S-δ for the interaction in singlet states and G_S for the interaction in the octet states [1].)

IX. DISCUSSION

In this work we have calculated the energy of fifty-four $q\overline{q}$ states using the parameters listed in Table II. The parameters Λ_3, μ, and m_u were fixed at the outset and m_q, G_S, G_V, and κ were adjusted to fit the masses of the $\omega(782)$, $\omega(1420)$, $K(495)$, and $\phi(1020)$. There are three other parameters, δ, G_K, and G_{KA}. The parameter δ was chosen when fitting the $\eta(547)$ and $\eta'(958)$ mass values. That parameter is meant to take into account the effect of the gluon fields upon the singlet state η^0. The value of G_K was introduced to create a significant interaction in the $^1P_1$ states and G_{KA} was introduced to create significant $^3P_1$-$^1P_1$ mixing for the strange axial-vector mesons. (Without such terms, the standard NJL interaction has a very small interaction in $^1P_1$ states and quite small $^3P_1$-$^1P_1$ mixing.) We note that the parameters are largely determined from our study of the pseudoscalar and vector nonets. Therefore, our predictions for states such as the $K_0^*(1430)$, $a_1(1260)$, and $K^*(892)$ require no parameter fitting. Our prediction for the mass of the $a_0(980)$ is too high by about 80 MeV. However, the nonstrange scalar states are known to have quite strong coupling to channels such as $\pi\pi$, $K\overline{K}$, and $\pi\eta$, so that one can expect a significant shift in energy arising from the real part of the meson self-energy that describes the decay to the various open channels [11,13].

A particular advantage of our formalism is that we combine chiral symmetry, covariance, and a model of confinement in the same model. While our Lagrangian has chiral symmetry, the approximations made in our Minkowski-space calculations violate chiral symmetry to some degree. Since the properties of the $\pi(138)$ are very sensitive to small violation of chiral symmetry, we neglect confinement in that case. Alternately, the pion may be studied in a Euclidean momentum space, where it is easier to maintain exact chiral symmetry in the presence of a model of confinement [9].

In the present work, we have not emphasized the covariance of our formulation. That feature played an important

role in our studies of the decays of the $\pi(1300)$ to $\pi+\sigma$ and $\pi+\rho$ channels [2]. For example, if the $\pi(1300)$ is taken to be at rest, the final-state mesons (σ, ρ, or π) have finite three-momentum. Therefore, to describe the confinement vertex for these mesons, we have to make use of the covariance of the model. The decay amplitude then becomes independent of the frame chosen for its evaluation. We have also shown that the various vacuum polarization functions, such as $J^P(P^2)$, $J^V_{\mu\nu}(P^2)$, $J^S(P^2)$, and $J^A_{\mu\nu}(P^2)$, may be calculated in any Lorentz frame with the same result.

The extension of our Lagrangian to include gradient terms is a novel feature of our work. We consider this aspect of our work somewhat preliminary to a more complete study of the effects of such terms upon the full range of mesons. It remains to be seen whether our model can explain the decay widths of $K_1(1270)$ and $K_1(1400)$ to various open channels, such as $K^*+\pi$ and $K+\pi$.

There exist several approaches to the study of light mesons. A model for the calculation of radial excitations of mesons in a generalized NJL is presented in Ref. [14]. Also, extensive studies of hadron properties have been made using the global color model and we list several useful works in Ref. [15]. In addition, there is a body of work that makes use of the potential models of the kind that are used in the study of heavy mesons. That body of work is reviewed in Ref. [16].

The overestimate by about 200 MeV of the energy of the $K^*(1410)$ seen in Fig. 5 is quite a similar feature to that exhibited in Fig. 14 of Ref. [16], where theoretical and experimental values for meson masses are shown. [In Sec. 4.2.2 of Ref. [16], it is suggested that the low energy of the $2\ ^3S_1$ $K^*(1410)$, when compared to the shell-model prediction, may be due to the mixing of two states via decay channels that lowers the energy of one state and increases the energy of the other. Alternatively, we may suggest a large shift due to the real part of the meson self-energy that describes the effects due to the coupling of the $K^*(1410)$ to the various open channels.] We may note that our value for the mass of the $K_0^*(1430)$, given in the data tables as 1412 ± 6 MeV, is better than the predicted value given in Ref. [16], which is about 170 MeV too small.

There are various projects that may be carried out in the future. For example, we may extend our work to study the tensor mesons. Also a more complete treatment of the properties of the K_1 mesons may be made. Clearly, a very large number of meson decay widths may be calculated at one quark-loop order in our model.

ACKNOWLEDGMENTS

This work was supported in part by a grant from the National Science Foundation and by the PSC-CUNY Faculty Research Award Program.

[1] Bo Huang, Xiang-Dong Li, and C. M. Shakin, Phys. Rev. C **58**, 3648 (1998).
[2] L. S. Celenza, Bo Huang, and C. M. Shakin, Phys. Rev. C **59**, 1041 (1999).
[3] L. S. Celenza, Bo Huang, and C. M. Shakin, Phys. Rev. C **59**, 1030 (1999).
[4] L. S. Celenza, Bo Huang, and C. M. Shakin, Phys. Rev. C **59**, 1700 (1999).
[5] L. S. Celenza, Bo Huang, and C. M. Shakin, Phys. Rev. C **59**, 2814 (1999).
[6] For reviews of the NJL model, supplemented by the 't Hooft interaction, see S. P. Klevansky, Rev. Mod. Phys. **64**, 649 (1992); U. Vogl and W. Weise, Prog. Part. Nucl. Phys. **27**, 195 (1991).
[7] S. Klimt, M. Lutz, U. Vogl, and W. Weise, Nucl. Phys. **A516**, 429 (1990).
[8] Particle Data Group, R. M. Barnett *et al.*, Phys. Rev. D **54**, 1 (1996).
[9] L. S. Celenza, Xiang-Dong Li, and C. M. Shakin, Phys. Rev. C **55**, 1492 (1997).
[10] P. Jain and H. J. Munczek, Phys. Rev. D **48**, 5403 (1993); H. J. Munczek and P. Jain, *ibid.* **46**, 438 (1992); J. Praschifka, C. D. Roberts, and R. T. Cahill, *ibid.* **36**, 209 (1987); P. C. Tandy, Prog. Part. Nucl. Phys. **39**, 117 (1994).
[11] L. S. Celenza, Xiang-Dong Li, and C. M. Shakin, Phys. Rev. C **55**, 3083 (1997); **56**, 3326 (1997).
[12] M. Suzuki, Phys. Rev. D **47**, 1252 (1993).
[13] N. A. Törnquist, Z. Phys. C **68**, 647 (1995).
[14] M. K. Volkov and C. Weiss, Phys. Rev. D **56**, 221 (1997).
[15] P. Maris and C. D. Roberts, Phys. Rev. C **56**, 3369 (1997); P. Maris, C. D. Roberts, and P. Tandy, Phys. Lett. B **420**, 267 (1998); C. J. Burden, Lu Qian, C. D. Roberts, P. Tandy, and M. J. Thompson, Phys. Rev. C **55**, 2649 (1997); M. R. Frank and C. D. Roberts, *ibid.* **53**, 390 (1996); C. D. Roberts, Nucl. Phys. **A605**, 475 (1996); C. D. Roberts and A. G. Williams, Prog. Part. Nucl. Phys. **33**, 477 (1994).
[16] S. Godfrey and J. Napolitano, ''Light Meson Spectroscopy,'' LANL archive: hep-ph/9811410 (1998).